Two-dimensional mapping of the electron density in laser-produced plasmas

Mathew Polek, Sivanandan S. Harilal,* and A. Hassanein

School of Nuclear Engineering and Center for Materials under Extreme Environment, Purdue University, West Lafayette, Indiana 47907, USA

*Corresponding author: hari@purdue.edu

Received 1 September 2011; revised 21 October 2011; accepted 24 October 2011; posted 27 October 2011 (Doc. ID 153623); published 27 January 2012

We performed two-dimensional (2D) mapping of the electron density in a laser-produced plasma with high spatial and temporal resolution. The plasma was produced by irradiating an aluminum target with 1064 nm, 6 ns pulses from a Nd:YAG laser under vacuum conditions. Stark broadening of the lines was used to estimate the electron density at various locations inside the plasma. The 2D spectral images were captured at different spatial points in the plasma using an imaging spectrograph coupled to an intensified CCD at various times during the plasma expansion. A comparison between radially averaged and radially resolved electron density profiles showed differences in the estimated values at the earlier times of plume evolution and closer distances to the target. However, the measured radially averaged values are consistent with 2D radial profiles at later times and/or farther distances from the target surface.

OCIS codes: 140.0140, 300.6550, 110.0110.

1. Introduction

Laser-produced plasmas (LPPs) have been the focus of extensive basic research that has led to a diverse range of applications in many domains, including pulsed laser deposition [1,2], elemental characterization using laser-induced breakdown spectroscopy [3–7], and short wavelength light sources [8]. LPP parameters are strongly dependent upon several key parameters, including laser intensity [9], laser pulse duration and wavelength [10,11], target material and geometry [12,13], and the nature and pressure of ambient gases [14]. The plasma characteristics also vary drastically with distance from the target surface both in the plume expansion direction (axial) and orthogonal to plume expansion directions (radial), as well as with time following the onset of plume formation.

The electron density (n_e) constitutes one of the most fundamental parameters of plasmas, and for many plasma systems, density varies more rapidly compared to any other plasma parameters, such as electron temperature (t_e) [15–20]. The distribution of electron density can provide information about the dynamics and evolution of the plasma. This information can then be used for various purposes, i.e., modeling processes in hydrodynamics, plasma physics, and plume expansion. Standard plasma diagnostic tools employed for the estimation of electron density are optical emission spectroscopy, the Langmuir probe, microwave and laser interferometry, and Thomson scattering [21]. Optical emission spectroscopy (OES) is routinely used for estimating the basic properties of the plume. Moreover, OES is a simple nonintrusive method for diagnosing the plasma [21,22]. For performing OES, typically the light emission from the plasma is imaged onto the entrance slit of a spectrograph, where the properties of the plasma plume are averaged over the height of the plasma (radial direction) while maintaining spatial resolution in the plume expansion direction (axial direction) [2,23,24]. However, the plasma properties change dynamically in all directions, especially at

1559-128X/12/040498-06$15.00/0

early times. Hence, even though estimation of plasma properties is performed with high axial precision in the plume expansion direction, the averaging over the radial direction of the plasma will affect the uncertainty of the measurement.

Plasma electron density determination using Stark broadening [21,22,25–27] of spectral lines is a well-established technique in the range of electron number density 10^{15}–10^{18} cm^{-3}. For electron density estimation, Stark broadened profiles of isolated lines are routinely used with emissions averaged over the radial direction (spectrograph slit height) [12,28]. In this article, we investigated the uncertainty in one-dimensional (1D) averaging of the electron density along the radial direction at various spatial and temporal points during plume expansion. Stark broadened profiles of spectral lines were used for measuring the electron density. The 1D electron density profiles are obtained by traditional averaging over the radial direction, while two-dimensional (2D) profiles are generated by sampling the emission signal at various radial positions along the height of the plasma after a single laser pulse. Our results indicate that nonnegligible errors in the measured 1D electron density values occur during the early times of plasma evolution.

2. Experimental Setup

The details of the experimental scheme used in the presented work are given elsewhere [12]. For generating plasma, high-purity Al targets were irradiated with 1064 nm, 6 ns Gaussian pulses from a Nd:YAG Continuum Surelite III laser (maximum energy ~700 mJ and beam diameter ~10 mm). The Al target was in the form of a slab and was placed inside a stainless steel vacuum chamber with a base pressure of about 10^{-6} Torr and positioned on a x–y–z translator. This allowed us to refresh the surface after every reading to avoid local heating and cavity formation.

The Nd:YAG laser pulses were focused onto the Al target using an antireflection-coated $f/40$ plano–convex lens to produce a 1 mm spot. The spot size was measured using burn paper and cross calibrated using crater width measurement using a microscope. The beam energy was attenuated using a combination of polarizing cube and wave plate, resulting in a power density of 2 GW/cm^2 at the target surface. The emission from the plasma was collected and focused using two $f = 40$ cm lenses into the entrance slit of a 0.5 m Acton-Pro Czerny–Turner spectrograph with 1:1 image correspondence. The focusing lenses were translated to track the plasma expansion for spatial analysis of the plume. A Princeton PIMAX intensified CCD (ICCD) camera with 1024×1024 pixels with a pixel size of 13 μm × 13 μm coupled to the spectrograph was used as a detector. The camera was attached to a programmable delay generator to control the time delay between the laser pulse and the ICCD. The spectrograph and ICCD combination provided a maximum resolution of 0.025 nm using a 30 μm slit width and 1800 grooves/mm grating.

3. Results and Discussion

The interaction of a focused high-power laser with an Al target leads to the formation of a plasma. This plasma rapidly expands freely into a vacuum in a direction perpendicular to the target surface [29]. The emission from the plasma consists of a continuum radiation due to bremsstrahlung, as well as lines from specific transitions. At the early times of the Al plasma (< 50 ns), the continuum emission dominates over the line emission, causing difficulties in gathering accurate line emission profiles. However, at later stages of plasma expansion, line emission begins to dominate over continuum emission. The analysis of line emission can yield plasma properties such as electron density. For example, the width and intensity of a spectral line is useful for obtaining electron density and temperature information of a laser ablated plume [30,31].

We used broadened profiles of emission lines to estimate the electron density of the Al plume at 10^{-6} Torr. The selected Al^+ line for the electron density measurement is 466.3 nm ($3p^2$-$3s4p$). A typical image of an Al^+ line emitting at 466 nm is given in Fig. 1. For 1D measurement, the average intensity value obtained from 100 pixels in the center region (which is equivalent to 1.3 mm) was used for deducing electron density. The 1D profiles are obtained by traditional averaging over the radial direction, while 2D profiles are generated by sampling the emission signal at various radial positions along the height of the plasma after a single laser pulse.

The main mechanisms contributing to the broadening of the spectral lines are Stark, resonance, Doppler, and instrumental broadening. Doppler broadening occurs when the emitting species are Doppler shifted due to their relative velocities, with larger velocity distributions causing a larger broadening effect. Contributions due to Doppler broadening were calculated by $\Delta\lambda_D = \lambda v_z/c$, where λ is the

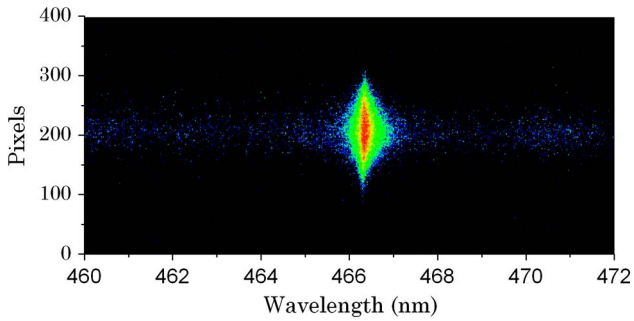

Fig. 1. (Color online) Emission resulting from 466.3 nm Al^+ line. Image is taken at a time of 50 ns and at a distance of 1 mm. For 1D measurement, the average intensity value obtained from 100 pixels in the center region (which is equivalent to 1.3 mm) was used for deducing electron density. For 2D measurement, the emission from 10 axial pixels (corresponding to 130 μm of the plasma height) was averaged at various radial distances.

wavelength of the line and v_z is the velocity of the emitting species. The determined expansion velocity of Al^+ species under similar irradiation conditions was $\sim 2 \times 10^6$ cm/s using time-of-flight optical emission spectroscopy [32], which corresponds to a Doppler broadening of ~0.03 nm. Doppler broadening is one of the major contributors for line broadening for emission far away from the target surface. The effect of resonance broadening is caused by collision between the emitting particle and an identical particle, resulting in an excitation from the ground state. Hence, resonance broadening is proportional to the ground state number density and the transition oscillator strength. The lower energy level of the selected line (466.3 nm) for electron density estimation is located at 10.6 eV and the reported transition probability [33] is 5.3×10^7 s^{-1}. The emitted lines may undergo self-absorption when the emitted photons are reabsorbed by the atom or the plasma. This effect is strongest on the peak of the emission line, which results in the appearance of a dip at the center. However, the 466.3 nm Al^+ line is not bound to the ground state of the atom and is known to have negligible self-absorption [34]. Moreover, the self-absorption in a spectral line is indicated by a spectral dip at the peak intensity region [35]. In our experiment, we have not noticed any spectral dip in the line center. The instrumental broadening, which is inherent in all spectrographs, can be minimized by lowering the slit width. The instrumental broadening can be calculated by the following equation [30]:

$$\Delta w_{1/2} = [(w_g^2 + (w_l/2)^2)]^{1/2} + w_l/2, \qquad (1)$$

where $\Delta w_{1/2}$ is the uncorrected full width at half-maximum (FWHM), w_g is the Gaussian width caused by instrument broadening, and w_l is the corrected value of the FHWM. Instrumental broadening was calculated to be about 0.025 nm when using a 30 μm slit width. Both Doppler and instrumental broadening are represented by Gaussian profiles.

In a plasma, Stark broadening is caused by collisions between the emitting species with charged particles, which perturb the transition levels of the emitting atom through variations in the electric field. Stark broadening is directly proportional to the electron density in a plasma and follows a Lorentz distribution. Our profiles are closely fitted to a Lorentz distribution, as shown in Fig. 2, meaning the effects from other broadening mechanisms are less significant. By analyzing the FWHM of the Stark broadened lines, it was possible to accurately calculate the electron density from the plasma using the equation [30,31]

$$\Delta\lambda 1/2 = 2\omega\left(\frac{n_e}{10^{16}}\right) + 3.5A\left(\frac{n_e}{10^{16}}\right)^{1/4}\left[1 - \frac{3}{4}N_D^{-1/3}\right]\omega\left(\frac{n_e}{10^{16}}\right)\text{Å}, \qquad (2)$$

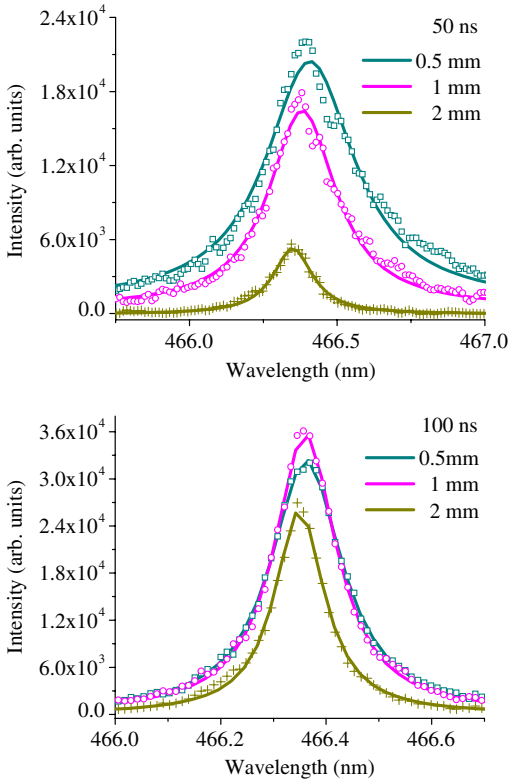

Fig. 2. (Color online) Examples of the Stark broadened profiles taken from 1D time-resolved spectra at 50 (top) and 100 ns (bottom) after the laser pulse. Solid points represent the experimental data and smooth curves are the Lorentz fits.

where $\Delta\lambda_{1/2}$ is the FWHM of Stark profiles, w is the electron impact parameter, n_e is the electron density, A is the ion impact parameter, and N_D is the number of particles in the Debye sphere. In Eq. (2), the two terms on the right side correspond to electron and ion contributions to the spectral broadening. However, the ion contribution to broadening is minimal in non-hydrogen plasmas [30] and contributes < 0.01 nm to the total broadening, allowing us to exclude it from our calculations to obtain Eq. (3):

$$\Delta\lambda 1/2 = 2\omega\left(\frac{n_e}{10^{16}}\right). \qquad (3)$$

For estimating the electron density, we used emission profiles of Al^+ at 466.3 nm and the impact parameter was obtained from [36–38]. The error associated with the impact parameter is typically ~10%–30%, which was not included in our error bars [37,38]. Figure 2 demonstrates the radially averaged Stark broadened profiles at various axial distances from the target and at different times after the plasma evolution. The solid curves in the figures are fitted to Lorentz distributions.

A. Radially Averaged 1D Density Measurements

Our goal in this experiment was to verify the errors associated with 1D averaging of the electron density. Figure 1 shows the emission resulting from 466.3 nm

Al^+ line passing through a 30 μm slit width of a Czerny–Turner spectrograph. The image was taken at a time of 50 ns and at a distance of 1 mm. For 1D measurement, the average intensity value obtained from 100 pixels in the center region (which is equivalent to 1.3 mm) was used for deducing electron density. A 1 μs gate width was used for the 1D time-integrated electron density measurements. The estimated radially averaged and time-integrated electron density of the plasma at various distances is given in Fig. 3. The instrumental broadening corrections were made using Eq. (1). The electron density followed a $1/z$ trend, as shown by the fitted curve in Fig. 3. However, the leveling of the electron density after 4 mm is unexpected, and can be attributed to the limitations of our instruments, as well as to a reduced rate of three-body recombination, which is directly proportional to the square of the electron density.

To explore errors due to time integration, we examined the radially averaged electron density variation with a time, and the results are given in Fig. 4 for various distances from the target surface. The gating time is incrementally increased from 10 to 60 ns to compensate the reduction in intensity with increasing distance. The fitted curves in Fig. 4 follow a $1/t$ dependence. There is a large difference in densities between the spatial and time-resolved plots which is caused by time integration. It should be remembered that laser plasma expansion is highly transient and fundamental parameters will vary rapidly with space and time [20,39]. In Fig. 4, it can be seen that the electron density drops much quicker for shorter axial distances, and the densities at every point become comparable after 150 ns. To evaluate the differences associated with radial averaging in the time-resolved plots, we performed 2D measurements. The results provide both space and time precision in the electron density measurements.

B. 2D Density Measurements

We inspected the densities of the plume in the radial direction to assess the differences with radially averaged 1D electron density measurement. The

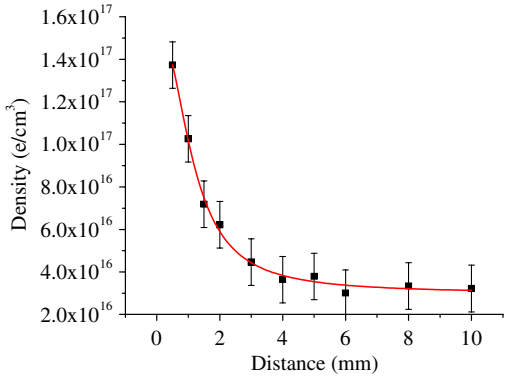

Fig. 3. (Color online) Electron density variation with distance from the target surface. The data is radially averaged and obtained with an integration time of 1 μs.

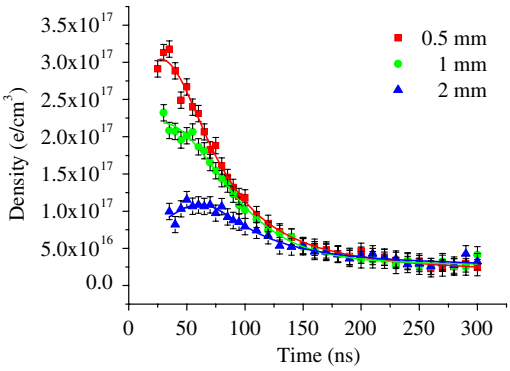

Fig. 4. (Color online) Time-resolved measurements of the electron density taken at 0.5, 1, and 2 mm. Points were taken from experimental data and solid curves are fitted to the data. The integration time is incrementally increased from 10 to 60 ns to compensate the reduction in emission intensity.

2D images of the plasma emissions were obtained at 50, 100, and 200 ns with integration times of 10, 20, and 40 ns, respectively, at various distances from target surface. To compensate for the lack of emission photons due to high space and time resolution, the images were recorded with an accumulation of five laser shots. The emission from 10 axial pixels (corresponding to 130 μm of the plasma height) was averaged at various radial distances to obtain the electron density. The radial profile of the electron density obtained at a distance of 1 mm from the target surface is shown in Fig. 5. This recorded radial profile shows good symmetry along the radial direction.

2D time-resolved measurements of the electron density obtained at 50, 100, and 200 ns after the laser pulse are given in Fig. 6. The electron density maintains symmetry across the radial distance at all times and distances. However, as the 2D profiles show, the electron density distribution changes considerably at recorded times after the laser pulse; it should be noted from the figure that the electron density gradient remained high in both the radial and axial directions, especially at earlier times. This gradient, particularly in the radial direction, leads to differences between the 1D and 2D electron density

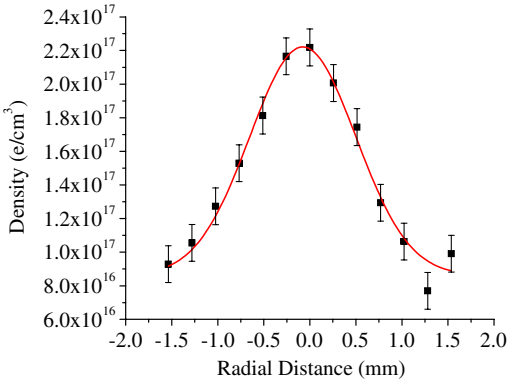

Fig. 5. (Color online) Radial profile of the density recorded at 50 ns and at a distance of 1 mm from the target surface.

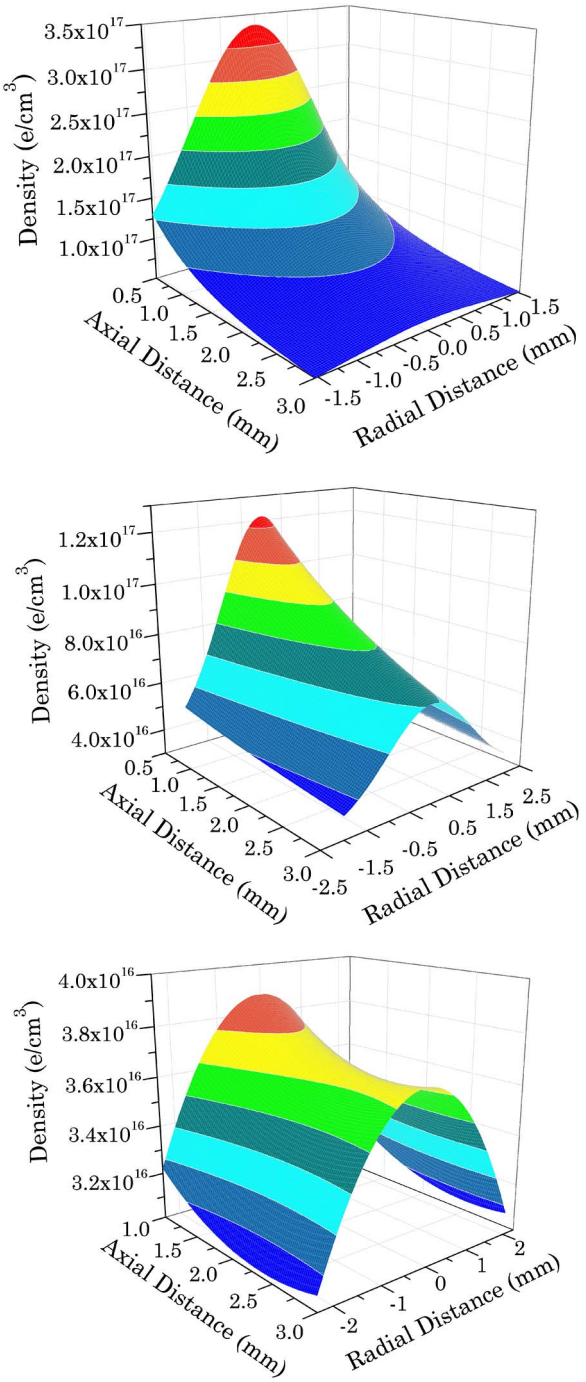

Fig. 6. (Color online) 2D time-resolved measurements of the electron density. 2D plots were taken at 50 (top), 100 (middle), and 200 ns (bottom) using 466.3 nm Al^+ line. A color scale is used to show regions of varying electron density. The integration times used are 10, 20, and 40 ns, respectively, for obtaining the density plots at 50, 100, and 200 ns.

measurements. For example, the maximum densities recorded for 2D measurements at 50 ns were 3.4×10^{17}, 2.2×10^{17}, and 1.3×10^{17} e/cm^3 at 0.5, 1, and 2 mm, respectively, in the plume expansion direction. In comparison, 1D electron density measurements at 50 ns showed 2.7×10^{17}, 2.0×10^{17}, and 1.1×10^{17} e/cm^3 at 0.5, 1, and 2 mm, respectively, which was 10%–20% lower than 2D electron densities. It should be mentioned that the line averaged electron density is estimated by binning 100 pixels, which corresponds to 1.3 mm in the radial direction. The changes in the electron density values will be much higher ($> 50\%$) if we use a 3 mm slit height, which is standard for most spectrographs. Eventually, as the electron density continued to decrease with time and space through expansion and recombination, the gradient in all directions began to disappear after 200 ns. Additionally, distances greater than 2 mm also had a nearly uniform electron density gradient at all times. From these results, it is reasonable to conclude that radially averaged electron density measurements closely match 2D measurements for distances > 2 mm and times > 200 ns for this experiment.

4. Conclusion

It is well known that LPPs are highly transient and its properties change rapidly with space and time. Typically, the fundamental parameters of laser plumes using emission spectroscopy were evaluated by line averaging along the slit height (radial averaging). We evaluated the differences in LPP electron density estimates between radially averaged and radially resolved electron density profiles. Stark broadening of line emission was used for measuring the electron density of Al plasma. A large electron density gradient was seen mostly at times earlier than 200 ns and at distances shorter than 3 mm. Hence, radially averaged 1D electron density measurements showed differences at earlier times of plasma evolution and/or closer distances from the target surface. However, at later times and farther distances, the measured radially averaged electron density values are consistent with 2D radial profiles.

This work was partially funded by the College of Engineering, Purdue University. The authors thank Khaled Al-Shboul for experimental help.

References

1. D. B. Chrisey and G. K. Hubler, *Pulsed Laser Deposition of Thin Films* (Wiley, 1994).
2. S. S. Harilal, "Spatial and temporal evolution of argon sparks," Appl. Opt. **43**, 3931–3937 (2004).
3. J. P. Singh and S. N. Thakur, *Laser-Induced Breakdown Spectroscopy* (Elsevier, 2007).
4. J. B. Ahmed and J. Cowpe, "Experimental and theoretical investigation of a self-absorbed spectral line emitted from laser-induced plasmas," Appl. Opt. **49**, 3607–3612 (2010).
5. C. Parigger, D. H. Plemmons, and J. W. L. Lewis, "Spatially and temporally resolved electron number density-measurements in a decaying laser-induced plasma using hydrogen-alpha line-profiles," Appl. Opt. **34**, 3325–3330 (1995).
6. V. N. Rai, H. S. Zhang, F. Y. Yueh, J. P. Singh, and A. Kumar, "Effect of steady magnetic field on laser-induced breakdown spectroscopy," Appl. Opt. **42**, 3662–3669 (2003).
7. A. K. Rai, V. K. Singh, V. Singh, S. N. Thakur, P. K. Rai, and J. P. Singh, "Quantitative analysis of gallstones using laser-induced breakdown spectroscopy," Appl. Opt. **47**, G38–G47 (2008).
8. V. Bakshi, *EUV Sources for Lithography* (SPIE, 2006).
9. S. S. Harilal, B. O'Shay, M. S. Tillack, Y. Tao, R. Paguio, A. Nikroo, and C. A. Back, "Spectral control of emissions from

tin doped targets for extreme ultraviolet lithography," J. Phys. D **39**, 484–487 (2006).
10. S. S. Harilal, R. W. Coons, P. Hough, and A. Hassanein, "Influence of spot size on extreme ultraviolet efficiency of laser-produced Sn plasmas," Appl. Phys. Lett. **95**, 221501 (2009).
11. D. Campos, S. S. Harilal, and A. Hassanein, "The effect of laser wavelength on emission and particle dynamics of Sn plasma," J. Appl. Phys. **108**, 113305 (2010).
12. R. W. Coons, S. S. Harilal, D. Campos, and A. Hassanein, "Analysis of atomic and ion debris features of laser-produced Sn and Li plasmas," J. Appl. Phys. **108**, 063306 (2010).
13. A. Hassanein, V. Sizyuk, T. Sizyuk, and S. Harilal, "Effects of plasma spatial profile on conversion efficiency of laser-produced plasma sources for EUV lithography," J. Micro/Nanolithog. MEMS MOEMS **8**, 041503 (2009).
14. S. S. Harilal, B. O'Shay, Y. Tao, and M. S. Tillack, "Ion debris mitigation from tin plasma using ambient gas, magnetic field and combined effects," Appl. Phys. B **86**, 547–553 (2007).
15. E. M. Monge, C. Aragon, and J. A. Aguilera, "Space- and time-resolved measurements of temperatures and electron densities of plasmas formed during laser ablation of metallic samples," Appl. Phys. A **69**, S691–S694 (1999).
16. J. A. Aguilera and C. Aragon, "Temperature and electron density distributions of laser-induced plasmas generated with an iron sample at different ambient gas pressures," Appl. Surf. Sci. **197**, 273–280 (2002).
17. D. Campos, S. S. Harilal, and A. Hassanein, "Laser wavelength effects on ionic and atomic emission from tin plasmas," Appl. Phys. Lett. **96**, 151501 (2010).
18. M. A. Bratescu, Y. Sakai, D. Yamaoka, Y. Suda, and H. Sugawara, "Electron and excited particle densities in a carbon ablation plume," Appl. Surf. Sci. **197**, 257–262 (2002).
19. B. Toftmann, J. Schou, T. N. Hansen, and J. G. Lunney, "Evolution of the plasma parameters in the expanding laser ablation plume of silver," Appl. Surf. Sci. **186**, 293–297 (2002).
20. D. W. Hahn and N. Omenetto, "Laser-induced breakdown spectroscopy (LIBS), Part I: review of basic diagnostics and plasma-particle interactions: still-challenging issues within the analytical plasma community," Appl. Spectrosc. **64**, 335A–366A (2010).
21. I. H. Hutchinson, *Principles of Plasma Diagnostics* (Cambridge University, 2002).
22. H. R. Griem, *Principles of Plasma Spectroscopy* (Cambridge University, 1997).
23. R. Noll, R. Sattmann, V. Sturm, and S. Winkelmann, "Space- and time-resolved dynamics of plasmas generated by laser double pulses interacting with metallic samples," J. Anal. At. Spectrom. **19**, 419–428 (2004).
24. J. A. Aguilera and C. Aragón, "Characterization of a laser-induced plasma by spatially resolved spectroscopy of neutral atom and ion emissions: comparison of local and spatially integrated measurements," Spectrochim. Acta B **59**, 1861–1876 (2004).
25. J. A. Aguilera, C. Aragon, and J. Bengoechea, "Spatial characterization of laser-induced plasmas by deconvolution of spatially resolved spectra," Appl. Opt. **42**, 5938–5946 (2003).
26. C. Aragon and J. A. Aguilera, "Determination of the local electron number density in laser-induced plasmas by Stark-broadened profiles of spectral lines: comparative results from H-alpha, Fe I and Si II lines," Spectrochim. Acta B **65**, 395–400 (2010).
27. M. Jedynski, J. Hoffman, W. Mroz, and Z. Szymanski, "Plasma plume induced during ArF laser ablation of hydroxyapatite," Appl. Surf. Sci. **255**, 2230–2236 (2008).
28. S. S. Harilal, B. O'Shay, M. S. Tillack, and M. V. Mathew, "Spectroscopic characterization of laser produced tin plasma," J. Appl. Phys. **98**, 013306 (2005).
29. C. Ursu, S. Gurlui, C. Focsa, and G. Popa, "Space- and time-resolved optical diagnosis for the study of laser ablation plasma dynamics," Nucl. Instrum. Methods Phys. Res. Sect. B **267**, 446–450 (2009).
30. N. M. Shaikh, S. Hafeez, B. Rashid, and M. A. Baig, "Spectroscopic studies of laser induced aluminum plasma using fundamental, second and third harmonics of a Nd:YAG laser," Eur. Phys. J. D **44**, 371–379 (2007).
31. H. R. Griem, *Principles of Plasma Spectroscopy* (Cambridge University, 1997).
32. K. F. Al-Shboul, S. S. Harilal, and A. Hassanein, "Gas dynamic effects on formation of dimers in laser-produced carbon plasmas," Appl. Phys. Lett. **99**, 131506 (2011).
33. NIST Atomic Spectra Database Lines Data, http://www.nist.gov/pml/data/asd.cfm.
34. G. Cristoforetti, "Orthogonal double-pulse versus single-pulse laser ablation at different air pressures: a comparison of the mass removal mechanisms," Spectrochim. Acta B **64**, 26–34 (2009).
35. R. C. Issac, S. S. Harilal, C. V. Bindhu, G. K. Varier, V. P. N. Nampoori, and C. P. G. Vallabhan, "Anomalous profile of a self-reversed resonance line from Ba+ in a laser produced plasma from $YBa_2Cu_3O_7$," Spectrochim. Acta B **52**, 1791–1799 (1997).
36. J. T. Knudtson, W. B. Green, and D. G. Sutton, "The UV-visible spectroscopy of laser-produced aluminum plasmas," J. Appl. Phys. **61**, 4771–4780 (1987).
37. E. Sarandaev and M. K. Salakhov, "Regularities in the stark widths and shifts of spectral lines of singly ionized Al," J. Quant. Spectrosc. Radiat. Transfer **56**, 399–407 (1996).
38. A. W. Allen, M. Blaha, W. W. Jones, A. Sanchez, and H. R. Griem, "Stark-broadening measurement and calculations for a singly ionized Al line," Phys. Rev. A **11**, 477–479 (1975).
39. M. A. Khater, J. T. Costello, and E. T. Kennedy, "Optimization of the emission characteristics of laser-produced steel plasmas in the vacuum ultraviolet: significant improvements in carbon detection limits," Appl. Spectrosc. **56**, 970–983 (2002).